NEOPLASIA
www.neoplasia.com

Volume 13 Number 5 May 2011 pp. 428–438 428

The Calcium-Sensing Receptor Is Necessary for the Rapid Development of Hypercalcemia in Human Lung Squamous Cell Carcinoma[1,2]

Gwendolen Lorch*, Serge Viatchenko-Karpinski†, Hsiang-Ting Ho†, Wessel P. Dirksen‡, Ramiro E. Toribio*, John Foley§, Sandor Györke† and Thomas J. Rosol‡

*Department of Veterinary Clinical Sciences, College of Veterinary Medicine, The Ohio State University, Columbus, OH, USA; †Dorothy M. Davis Heart & Lung Research Institute, The Ohio State University, Columbus, OH, USA; ‡Department of Veterinary Biosciences, College of Veterinary Medicine, The Ohio State University, Columbus, OH, USA; §Medical Sciences, Indiana University, Bloomington, IN, USA

Abstract

The calcium-sensing receptor (CaR) is responsible for the regulation of extracellular calcium (Ca^{2+}_o) homeostasis. CaR activation has been shown to increase proliferation in several cancer cell lines; however, its presence or function has never been documented in lung cancer. We report that Ca^{2+}_o-activated CaR results in MAPK-mediated stimulation of parathyroid hormone–related protein (PTHrP) production in human lung squamous cell carcinoma (SCC) lines and humoral hypercalcemia of malignancy (HHM) *in vivo*. Furthermore, a single nucleotide polymorphism in CaR identified from a hypercalcemia-inducing lung SCC reduced the receptor's activation threshold leading to increased PTHrP expression and secretion. Increasing the expression of either wild-type CaR or a CaR variant with a single nucleotide polymorphism in the cytoplasmic domain was both necessary and sufficient for lung SCC to induce HHM. Because lung cancer patients who frequently develop HHM and PTHrP expression in lung cancer has been only partially explained, the significance of our findings indicates that CaR variants may provide a positive feedback between PTHrP and calcium and result in the syndrome of HHM.

Neoplasia (2011) 13, 428–438

Introduction

Development of hypercalcemia of malignancy (HHM) results from dysregulated secretion of parathyroid hormone–related protein (PTHrP) typically in patients with epithelia-derived cancers. Studies from developed nations in the 1970s and 1980s, as well as recent studies from newly industrialized countries, report that patients with SCC of the lung have the highest frequency of HHM (ranging from 27% to 66%) compared with other tumor types [1]. Recently, we have identified mechanisms that activate high levels of PTHrP gene expression in human lung SCC lines that produce HHM in xenograft models [2,3]. In a subset of SCC lines capable of producing HHM, autocrine EGFR-signaling through the mitogen-activated protein kinase (MAPK) pathway induced high levels of PTHrP gene expression, whereas in other lung SCC lines, such gene activation was dependent on extrinsic host-derived factors [3].

The calcium-sensing receptor (CaR) is a central regulator of extracellular calcium (Ca^{2+}_o) homeostasis. The biochemical properties of CaR place it in the superfamily of G-protein–coupled receptors (GPCRs). The CaR is activated in response to certain extracellular stimuli such as Ca^{2+}, Mg^{2+}, and amino acids, which stimulate phospholipase C (PLC) to produce diacylglycerol and inositol 1,4,5-trisphosphate (IP_3). IP_3 stimulates Ca^{2+} release from the endoplasmic reticulum

Address all correspondence to: Gwendolen Lorch, DVM, PhD, Department of Veterinary Clinical Sciences, The Ohio State University, Goss Labs, 1925 Coffey Rd, Columbus, OH 43210. E-mail: gwendolen.lorch@cvm.osu.edu

[1]This study was possible with funding from the National Institutes of Health to G. Lorch (K01 RR021879) and S. Gyorke (R01 HL074045-09).

[2]This article refers to supplementary materials, which are designated by Tables W1 and W2 and Figures W1 to W5 and are available online at http://www.neoplasia.com.

Received 19 November 2010; Revised 9 February 2011; Accepted 10 February 2011

DOI 10.1593/neo.101620

and activates signal transduction pathways, such as mitogen-activated protein kinase–extracellular signal–related kinases (MAPK-ERK) and MAPK–cJun–N-terminal kinase (JNK), whereas diacylglycerol activates protein kinase C (PKC) [4]. Signaling by CaR is negatively regulated, in part, by PKC-mediated phosphorylation of a threonine in the intracellular domain (Thr^{888}) [5,6]. Phosphorylation of this PKC site inhibits activation of PLC by CaR and, therefore, serves as a negative feedback system.

The CaR regulates calcium homeostasis by inhibiting parathyroid hormone secretion from the parathyroid chief cells and activating Ca^{2+} reabsorption from the kidney thick ascending limb. The CaR is one of just a few GPCRs where genetic mutations have been linked with disease. For example, homozygous inactivating mutations of *CaR* are responsible for neonatal severe hyperparathyroidism, which results in severe hypercalcemia due to marked hyperparathyroidism, secondary skeletal demineralization, and subsequent pathological fractures [7]. The CaR is expressed in tissues beyond those directly involved in mineral homeostasis such as the brain, pancreas and lens epithelium. One function of CaR (at a nonparathyroid site) is physiological regulation of PTHrP secretion by breast tissue [8].

Disruptions in calcium-mediated signaling pathways are well-established features in the genesis and progression of cancer [9]. The disturbance of calcium regulation in many lung SCC patients suggests that CaR activation may contribute to altered intracellular calcium (Ca^{2+}_i) signaling in the tumor or its microenvironment. Recent work has detected CaR expression in adult lungs [10]; however, it is unknown if CaR is present in human lung cancer or if it contributes to the regulation of PTHrP expression and secretion.

In this report, we detected the expression of CaR in three human lung SCC lines. In addition, we documented that CaR regulated PTHrP gene expression and secretion *in vitro*. By using a xenograft lung SCC model of HHM with a knockdown of CaR, we showed that CaR was required for the rapid development of HHM. Furthermore, we demonstrated the presence of CaR single nucleotide polymorphisms (SNPs) in two lung SCC lines, HEK293T cells and human lung SCC samples. Finally, we established that overexpression of the CaR SNP R990G interfered with PKC-mediated feedback of receptor signaling and was sufficient to induce HHM in a normocalcemic xenograft model of lung SCC.

Materials and Methods

Cell Culture

The human RWGT2 SCC cell line was obtained from Drs G. Mundy and T. Guise (University of Texas Health Science Center, San Antonio, TX, and Indiana University School of Medicine, Indianapolis, IN). The human HARA SCC cell line was obtained from Dr Haruo Iguchi (National Cancer Center Research Institute, Tokyo, Japan). The human BEN cell line was obtained from Dr T.J. Martin (Brisbane, Australia) and was originally established from a hypercalcemic patient with an SCC of the bronchus [11]. Transformed human embryonic kidney 293 cells No. CRL-11268 (293T/17) at cell passage 12 were purchased from American Type Culture Collection (Manassas, VA). All cell lines were authenticated by the Johns Hopkins Genetic Resources Core Facility on October 26, 2010. Purified genomic DNA was submitted for STR analysis using AmpF/STR Identifiler (Applied Biosystems, Carlsbad, CA). Cell lines were maintained in high-glucose Dulbecco modified Eagle medium (DMEM) with GlutaMax (Invitrogen, Carlsbad, CA), supplemented with 10% heat-inactivated fetal bovine serum (FBS) at 37°C and 5% CO_2. Cells were passaged at 90% confluence. *In vitro* experiments, with the exception of Ca^{2+}_i release studies, were performed when RWGT2, HARA, BEN, and HEK293T cells were ~80% to 90% confluent.

Human Lung Biospecimens

Human lung biospecimens were provided by the eastern, midwestern, and western divisions of the Cooperative Human Tissue Network. Other investigators may have received specimens from the same subjects. The research project was approved by the institutional review board of The Ohio State University. Tissue specimens were registered in their respective biobanks and kept anonymous. Both nonaffected lung (NAT) and the primary lung squamous cell tissues (SCC) were obtained for each patient sample (n = 40). No patients had prior chemotherapy or radiation treatment. The biospecimens were diagnosed as lung SCC and staged by histopathologic analysis.

Generation of shRNA-CaR, BEN, RWGT2, and HARA Cell Lines

Briefly, 5×10^4 BEN, RWGT2, and HARA cells were seeded in a 12-well culture plate. Cells were transduced with SMARTvector short hairpin RNA (shRNA) Lentiviral Particles, SMARTvector Empty-Vector Control Particles or SMARTvector 2.0 Non-Targeting Control Particles (Thermo Fisher Scientific, Lafayette, CO) at an MOI of 40. Lentiviral particles used were as follows: a set of three different shRNA constructs targeting CaR, GAPDH, an empty-vector expressing TurboGFP, or a nontargeting negative control vector (scrambled CaR sequence) expressing TubroGFP. Seventy-two hours after initial transduction, gene knockdown was assessed by reverse transcription–polymerase chain reaction (RT-PCR) of total cellular complementary DNA (cDNA) and real-time confocal microscopy. Selection for the maximally silenced shRNA-CaR cells in all three lung SCC lines was achieved by FACS analysis from which a 1×10^4 population of cells with the greatest fluorescent reporter function were selected for use in additional studies.

Real-time Confocal Laser scanning Microscopy for Determination of Ca^{2+}_i

Determination of Ca^{2+}_o-induced changes in Ca^{2+}_i was done by loading the lung SCC lines with Ca^{2+}-sensitive fluorescence probes, fluo-3AM, or rhod-2AM for GFP-expressing cell lines (Molecular Probes, Carlsbad, CA). Ca^{2+}_i dynamics in single cells was measured as previously published [12].

PTHrP Analysis

PTHrP (1-86) concentrations in plasma and cell culture–conditioned media were measured using a commercially available two-site immunoradiometric assay (Diagnostic Systems Laboratories, Houston, TX).

Xenografts in Nude (Foxn1^{nu}) Mice and Biochemical Analysis

All experimental procedures were approved by The Ohio State University Institutional Laboratory Animal Care and Use Committee. Tumors were grown, and hypercalcemia was monitored as

described [3]. Plasma and total calcium concentrations ([Ca^{2+}]) were measured using the Vitros DT-60 II clinical chemistry analyzer (Johnson & Johnson, Ramsey, MN). Animals were considered hypercalcemic when total plasma [Ca^{2+}] were ≥12 mg/dl.

Statistics

Results were expressed as the mean ± SEM of triplicate or quadruplicate measurements with the exception of the PTHrP secretions studies in which the results were expressed as mean ± SD and compared with the two-tailed Student's *t* test. A probability value of $P < .05$ was considered to be significant. Analyses of variance (ANOVAs) were used to analyze the time differences between groups. If the equal-variance test failed when comparing multiple groups, a Kruskal-Wallis one-way ANOVA on ranks followed by the Dunn method of multiple comparison was used to analyze differences in tumor volume and [Ca^{2+}]. Plots with the variable time in the *x* axis are reported to show the trends over time (SigmaPlot 11, Chicago, IL).

Results

CaR mRNA and Protein Were Expressed in Human Lung SCC Lines

RT-PCR and Western blots were used to detect CaR mRNA and protein in three lung SCCs (BEN and HARA derived from primary pulmonary tumors and RWGT2 derived from a bone metastasis). All lines have been reported to express moderate to high levels of PTHrP [13–15], but only HARA and RWGT2 produce hypercalcemia in mice. Structure-function relationships of CaR have been traditionally studied using the putatively receptor-negative HEK293 cells. Positive controls for CaR expression included the receptor transfected HEK293 line, kidney, as well as breast and prostate cancer lines [16]. The CaR product was amplified from the cDNA of all lung SCC lines and surprisingly the HEK293T cell line (Figure 1*A*). An immunoreactive band was detected at 130 kDa in HEK293T cells and all lung SCC extracts on Western blots, similar to the mannose-modified intracellular form of CaR present in human whole kidney lysate (Figure 1*B*).

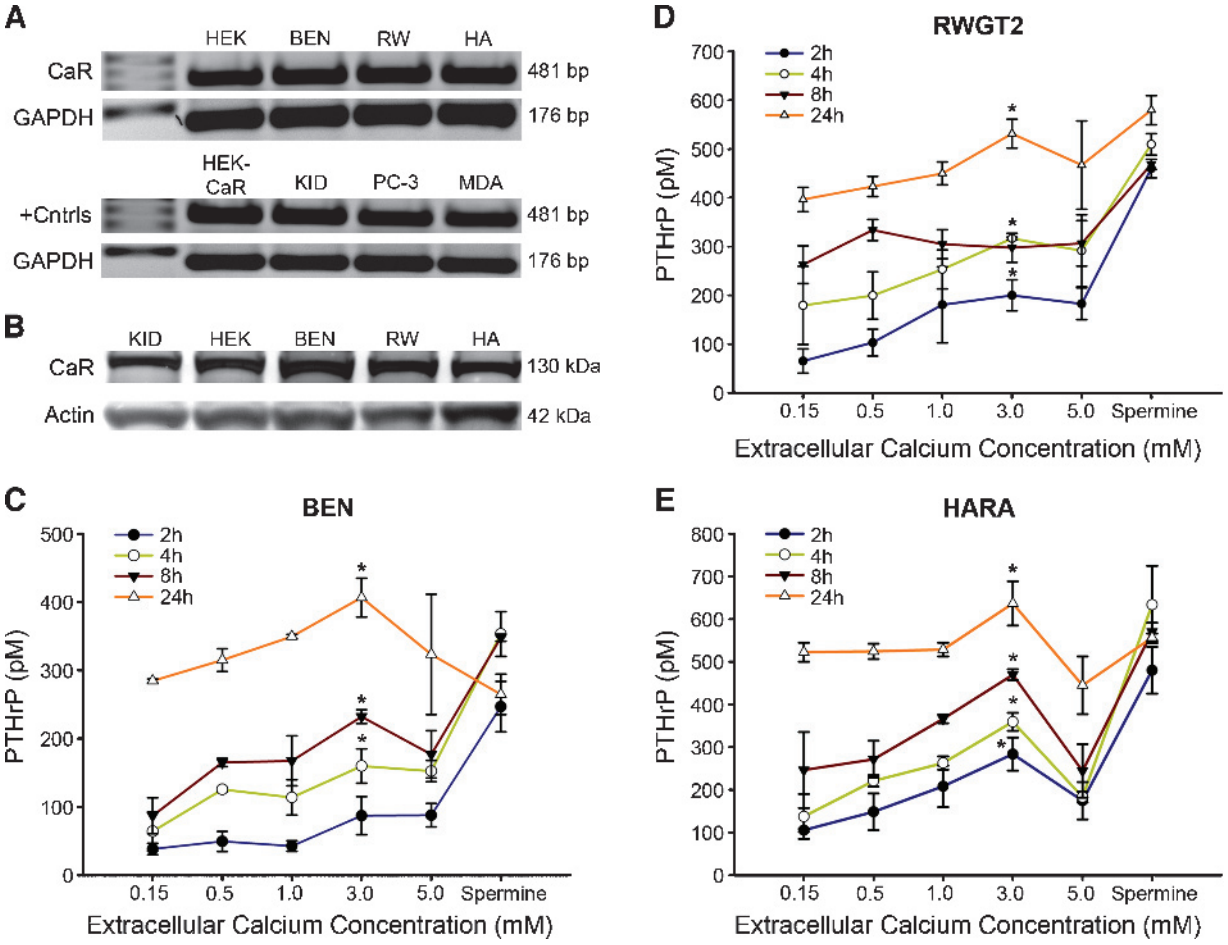

Figure 1. CaR mRNA and protein expression in lung SCC cells and the effect of $[Ca^{2+}]_o$ on PTHrP secretion. (A) RT-PCR amplification of CaR from HEK293T (HEK) (historical negative control for CaR expression) (lane 2), BEN, RWGT2 (RW), and HARA (HA) lines and positive controls (+Cntrls) CaR-transfected HEK293T (HEK-CaR) (lower lane 2) human kidney tissue (KID), the PC-3 prostate carcinoma cells (PC-3), and the breast cancer line, MDA-MB-231(MDA). Lane 1 is a ladder. CaR-specific human primers amplified a single 481-bp product in all cell lines including HEK293T. (B) Relative CaR expression by Western blots of cell extracts from adult human kidney (KID) (+ control) lane 1, HEK293T cells (HEK) from ATCC lane 2, and lung SCCs. Experiments were repeated three times and data from a representative blot are shown. (C–E) PTHrP secretion after treatment with increasing [Ca^{2+}] or spermine (2.0 mM). CaR activation increased [PTHrP] at all time points with an EC_{max} of approximately 3.0 mM Ca^{2+} excluding spermine treatments. Each value is the mean ± SD of three experiments. *Significant difference between treatment and cells grown in 0.15 mM (*$P < .05$ *vs* 0.15 mM).

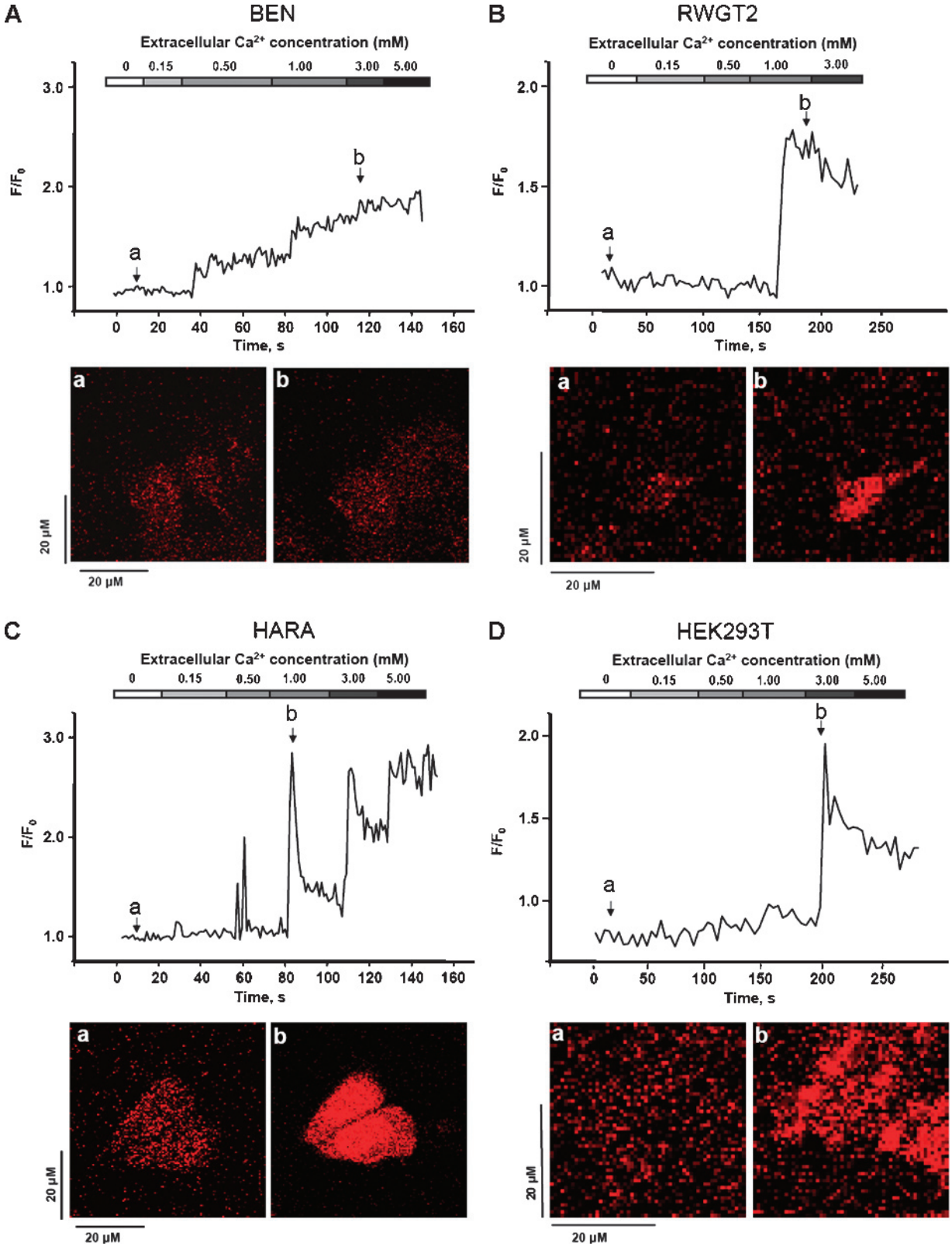

Figure 2. Increasing $[Ca^{2+}]_o$ induced a biphasic $Ca^{2+}{}_i$ rise in lung SCC cells. (A–D) The graphs are representative of fluo-3 fluorescent $Ca^{2+}{}_i$ responses observed in typical experiments using each lung SCC line and HEK293T cells. $Ca^{2+}{}_i$ baseline was measured in 0.0 mM Ca^{2+} solution, and $Ca^{2+}{}_i$ oscillations were initiated by the addition of 0.15 mM Ca^{2+}. The panels below are confocal microscopy images depicting fluo-3–loaded cells at baseline (a) and subsequent emittance of fluorescence on stimulation with $Ca^{2+}{}_o$ (b). Magnification, ×10.

Treatment with Ca^{2+}_o Increased PTHrP mRNA Expression and Secretion

Cell viability of the three lung SCCs lines was assessed after 24 hours to increasing $[Ca^{2+}]_o$ or spermine, a potent CaR activator. No significant effect on cell viability of any of the lung SCCs was found (Figure W1, *B–D*). Cells were treated with increasing $[Ca^{2+}]_o$ and 2.0 mM spermine for PTHrP mRNA expression and protein secretion studies. The concentrations of Ca^{2+}_o were selected to range from the serum-ionized calcium of a normal patient, 4 mg/dl (1.0 mM) through those equivalent to a patient with HHM, 12 mg/dl (3.0 mM) and levels toxic to normal human tissues 5.0 mM. Figure W2 shows that treatment of all three lung SCC lines with 3.0 mM Ca^{2+} resulted in statistically significant increases in PTHrP/GAPDH mRNA ratios at all but one time point. A significant stimulation of PTHrP secretion at 3.0 mM Ca^{2+} *versus* 0.15 mM was present in all cell lines at the majority of time points (Figure 1, *C–E*). PTHrP secretion after treatment with 3.0 mM Ca^{2+} was generally greater than with 5.0 mM. These data demonstrated that PTHrP expression and secretion could be increased by elevated Ca^{2+}_o levels.

Our data implicate CaR as a regulator of PTHrP secretion in lung SCC. The frequency of Ca^{2+}_i oscillations has been linked to changes in gene expression [17,18]; therefore, we hypothesized that stimulation of CaR and the resulting Ca^{2+}_i release as represented by either oscillation frequency or amplitude may account for the differences in PTHrP expression. We used real-time confocal microscopy to measure Ca^{2+} released from intracellular stores. BEN cells exhibited a gradual increase in Ca^{2+}_i (Figure 2*A*), whereas RWGT2 cells did not respond until stimulation with 1.0 mM Ca^{2+}_o when an abrupt increase in Ca^{2+}_i occurred (Figure 2*B*). The HARA cells displayed vigorous concentration-dependent oscillations of Ca^{2+}_i with a maximum F/F_0 ratio of approximately 2.5 when stimulated with 1.0 mM Ca^{2+}_o (Figure 2*C*). Importantly, when the HARA cells were treated

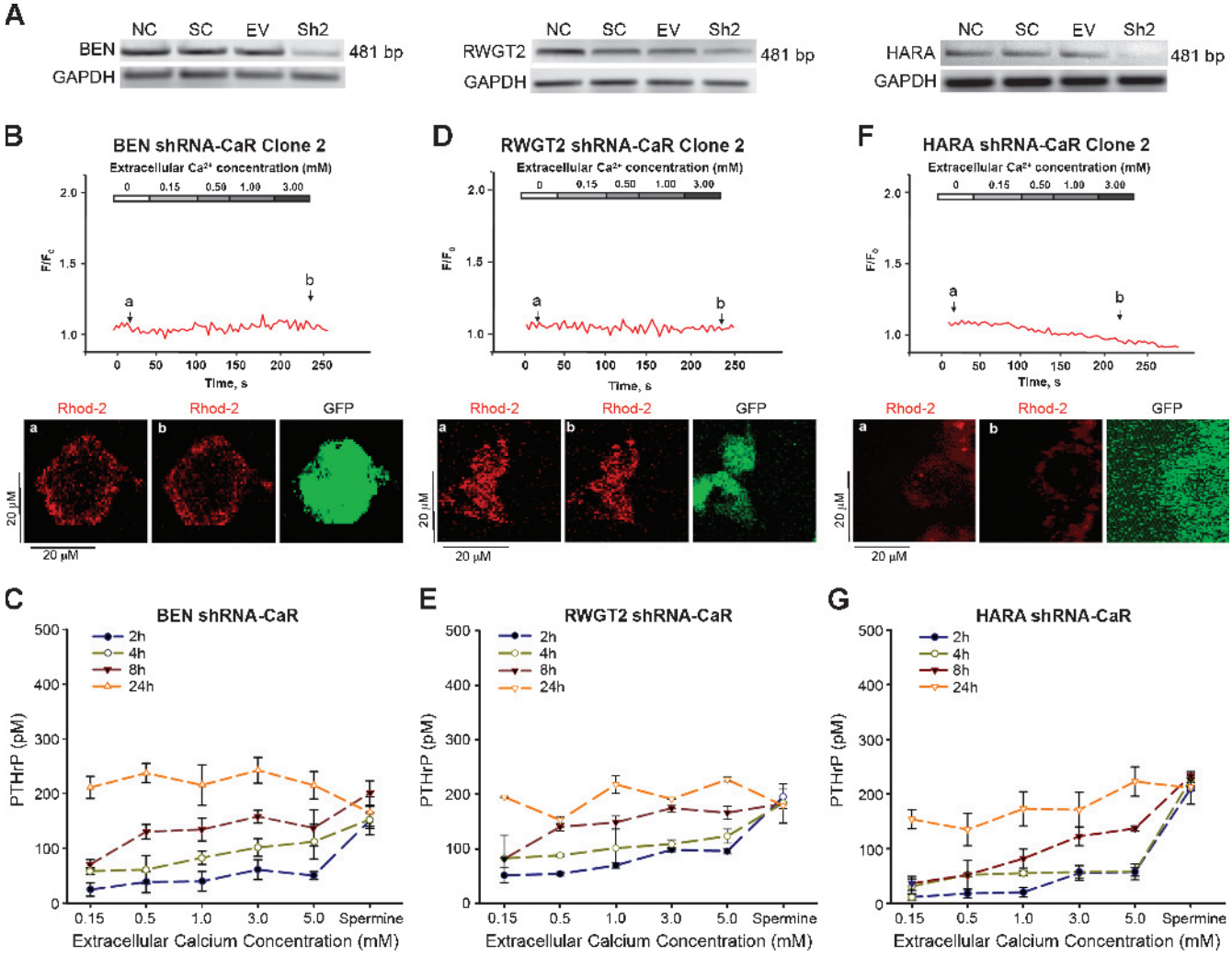

Figure 3. shRNA-CaR reduced CaR mRNA expression, PTHrP secretion, and Ca^{2+}_i release. (A) RT-PCR detection of CaR from SCC lines transduced with lentiviral shRNA to CaR (Sh2), scrambled-control RNA (SC), empty-vector (EV), or nontransduced (NC). (B, D, F) The graphs are representative of rhod-2 fluorescent Ca^{2+}_i responses from each shRNA-CaR line. The panels below Ca^{2+}_i response curves labeled (a, b) are confocal microscopy images depicting rhod-2–loaded cells at baseline before stimulation (a) and after stimulation with 3.0 mM Ca^{2+}_o in the same cell (b) the third panel depicts GFP expression from the transduced vector. The shRNA-CaR lines had reduced PTHrP secretion (C, E, and G). Reduction of PTHrP secretion was 31%, 55%, and 74% for BEN (Figure 1C *vs* Figure 3C), RWGT2 (Figure 1D *vs* Figure 3E), and HARA (Figure 1E *vs* Figure 3G), respectively.

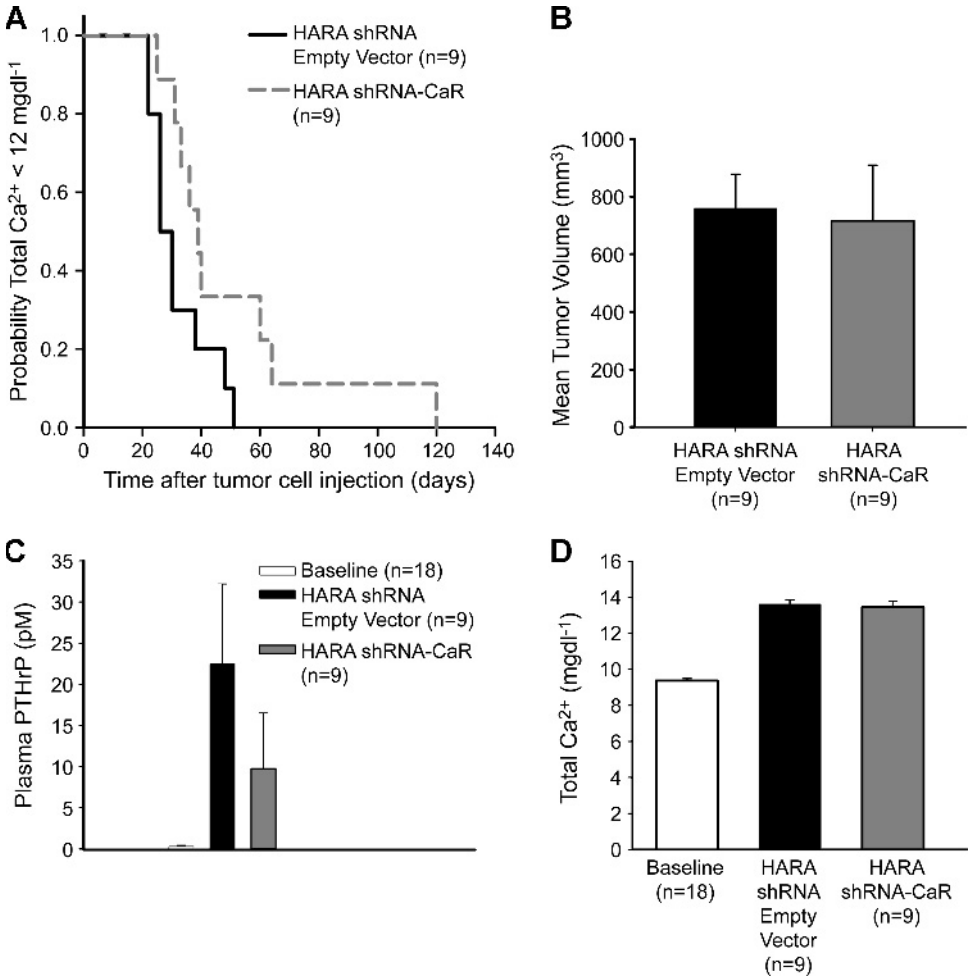

Figure 4. The CaR was necessary for the rapid development of HHM in the HARA xenograft model. (A) Kaplan-Meier analysis indicated HHM developed more rapidly in HARA shRNA empty-vector mice than HARA shRNA-CaR ($P = .023$). (B) Average tumor volume at the time of hypercalcemia. (C) Average plasma [PTHrP] in the HARA shRNA empty-vector mice were 190% greater (23 *vs* 8.0 pM) compared to the HARA shRNA-CaR mice ($P = .11$). (D) Comparison of plasma total [Ca^{2+}] in HARA shRNA empty-vector and HARA shRNA-CaR mice before xenografting (baseline) and at the time of HHM. No differences were observed.

with just 0.5 mM Ca^{2+}_o, a two-fold increase in Ca^{2+}_i occurred, an intensity that was greater than the fold increase achieved by either the BEN or RWGT2 lines. The significantly greater intensity in fluorescence acquired at a lower $[Ca^{2+}]_o$ in HARA can be described as shifted to the left when compared to other lines, suggesting a potential for differential signaling downstream from the receptor.

Inhibition of CaR Expression Reduced Ca^{2+}_i Mobilization and PTHrP Gene Expression, Delaying the Onset of HHM

To further characterize the role of CaR in the SCC lines, we knocked down endogenous CaR using a lentiviral short-hairpin interfering RNA (shRNA-CaR) and examined gene expression for CaR and its signaling (Figure 3*A*). Transduction of shRNA-CaR reduced CaR in all lung SCC lines and markedly decreased Ca^{2+}_o-induced Ca^{2+}_i responses (Figure 3, *B*, *D*, and *F*). These data support the conclusion that Ca^{2+}_i oscillations are Ca^{2+}-dependent through the activation of CaR.

The results from the Ca^{2+}_o stimulation studies indicated that Ca^{2+}_o may have activated PTHrP secretion in the lung SCC lines via the CaR. PTHrP secretion in response to $[Ca^{2+}]_o$ and spermine in the shRNA-lung SCC CaR clones was measured and found to be reduced in all three lines (Figure 3, *C*, *E*, and *G*). These results definitively demonstrated that CaR was necessary for lung SCC cells to secrete high levels of PTHrP in response to elevated Ca^{2+}_o.

We investigated whether CaR was required for the development of HHM in lung SCC by comparing the time to development of hypercalcemia between a xenograft mouse model of HARA carrying a shRNA empty-vector clone and mice carrying the HARA shRNA-CaR clone. The Kaplan-Meier long rank survival analysis revealed a significant difference ($P = .023$) between the groups when hypercalcemia was identified (i.e., the time point represents the very first day HHM was identified and therefore the date of euthanasia). The HARA shRNA empty-vector line produced hypercalcemia in less time after tumor cell injection than the HARA shRNA-CaR cells (50% of the HARA shRNA empty-vector mice were hypercalcemic in 29 days *vs* HARA shRNA-CaR in which 50% of the mice were hypercalcemic in 49 days) as shown in Figure 4*A*. Moreover, there were no differences found in tumor volume or weight (data not shown) between the HARA shRNA empty-vector and HARA shRNA-CaR groups (Figure 4*B*), which indicates that the increased time to development of HHM was not due to altered growth of the

shRNA-CaR tumors. The results suggested that CaR was necessary for the rapid development of HHM in the HARA xenograft model.

Decreased Immunohistochemical Expression of CaR and PTHrP in Lung SCC Xenograft Tumors from HARA shRNA-CaR Mice

The immunoreactivity of CaR and PTHrP was investigated in xenograft tumors derived from mice injected with either the HARA shRNA empty-vector or the HARA shRNA-CaR clone. The phosphoCaR antibody produced a specific and robust cytoplasmic and nuclear signal (Figure W3, *A* and *B*), whereas the PTHrP antibody produced a moderately intense diffuse, finely granular cytoplasmic, and sparse nuclear pattern in lung SCCs from the HARA shRNA empty-vector tumor (Figure W3, *C* and *D*). Both phosphoCaR- and PTHrP-positive reactions were successfully blocked with their respective blocking peptides. A significant decrease in staining intensity was evident for both the phosphoCaR and PTHrP antibodies in the lung SCC tumors from the HARA shRNA-CaR group. The phosphoCaR staining distribution was strikingly decreased in the cytoplasm and barely detectable in the nucleus (Figure W3, *E* and *F*). PTHrP antibody staining remained primarily localized to the cytoplasm and was markedly reduced (Figure W3, *G* and *H*). The results of the immunohistochemistry confirm that use of shRNA to silence CaR expression in HARA lung SCCs decreases both CaR protein and downstream PTHrP production. The specificities of the primary phosphoCAR and PTHrP antibodies were further evaluated on normal human adult lung tissue sections. In accordance with the work of Milara et al. [10], the phosphoCaR antibody staining pattern showed detection of CaR in a pulmonary artery and bronchi (Figure W3*I*) in lung parenchyma and type 2 pneumocytes (Figure W3*J*). Furthermore, PTHrP was located on the endothelial venules, capillaries (Figure W3*K*) and in nuclei of type 2 pneumocytes (Figure W3*L*), exclusive locations in which PTHrP has been detected previously in the adult lung [19,20].

Altered CaR Signaling in HARA Cells

Our findings of the dependence of PTHrP secretion on CaR and a leftward-shifted $Ca^{2+}{}_i$ mobilization response to $Ca^{2+}{}_o$ suggested that the HARA line may exhibit an overall gain-of-function downstream

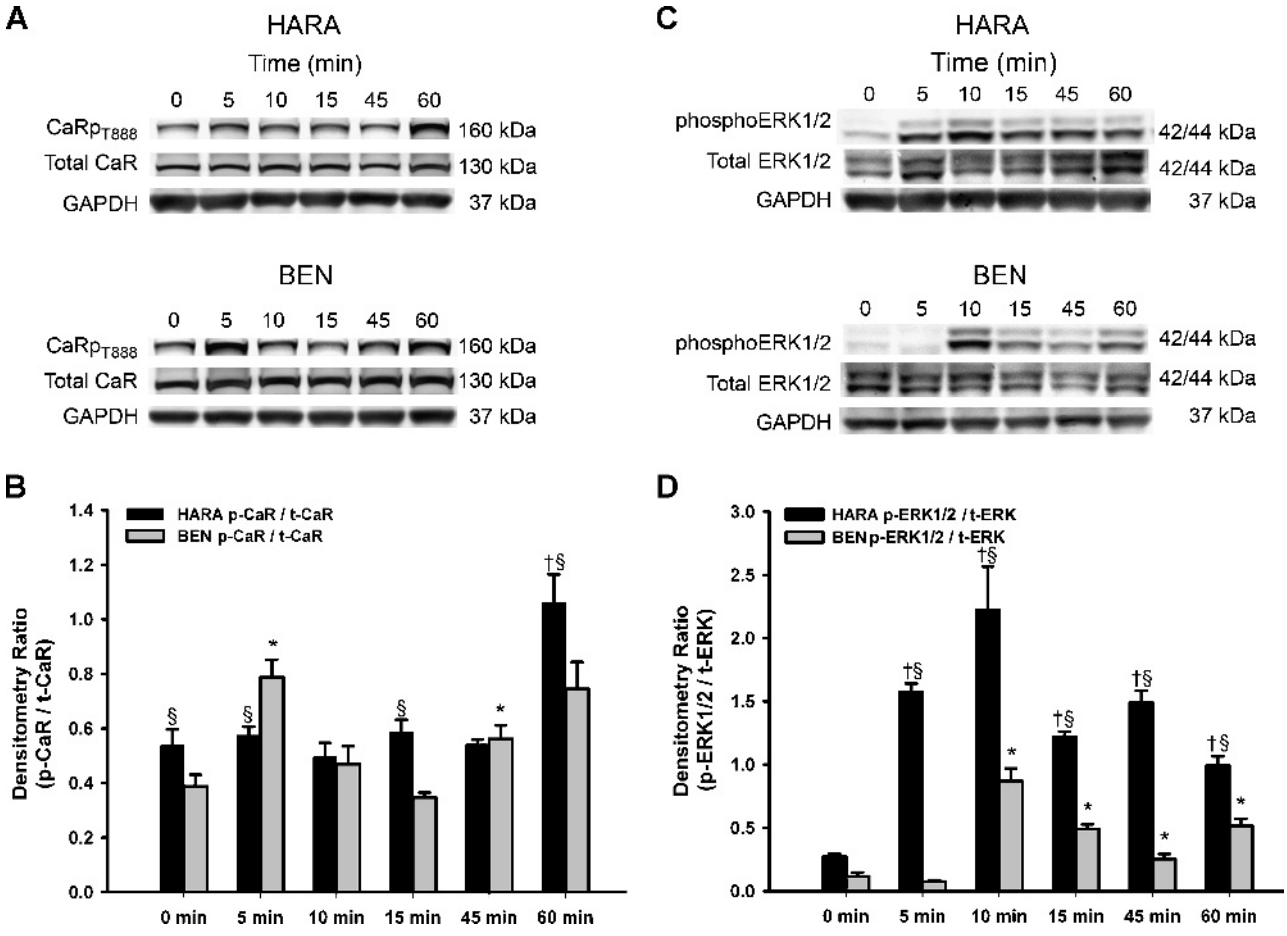

Figure 5. $Ca^{2+}{}_o$ induced CaR phosphorylation at threonine 888 and ERK1/2 phosphorylation. (A) Western blots of protein lysates from 5.0 mM Ca^{2+} treated BEN and HARA cells at various time points probed with CaR^{T888} phosphorylation-specific antibody. GAPDH Western blot serves as a loading control. (B) Densitometry: the levels of phosphorylated CaR were normalized to total CaR and GAPDH. Results were from three experiments. Bars, SEM. *BEN p-CaR/t-CaR: $P < .05$, compared to 0 time point. †HARA p-CaR/t-CaR: $P < .05$, compared to 0 time point. §BEN p-CaR/t-CaR *versus* HARA p-CaR/t-CaR: $P < .05$. (C) Western blots of protein lysates from 3.0 mM Ca^{2+}–treated BEN and HARA cells at various time points probed with antibodies against ERK1/2 phosphorylation, total ERK, and GAPDH. (D) Quantitative analysis by densitometry. The levels of phosphorylated ERK1/2 were normalized to total ERK and GAPDH as above. Bars, SEM. *BEN p-ERK1/2/t-ERK: $P < .05$, compared to 0 time point. †HARA p-ERK1/2/t-ERK: $P < .05$, compared to 0 time point. §BEN p-ERK1/2/t-ERK *versus* HARA p-ERK1/2/t-ERK: $P < .05$.

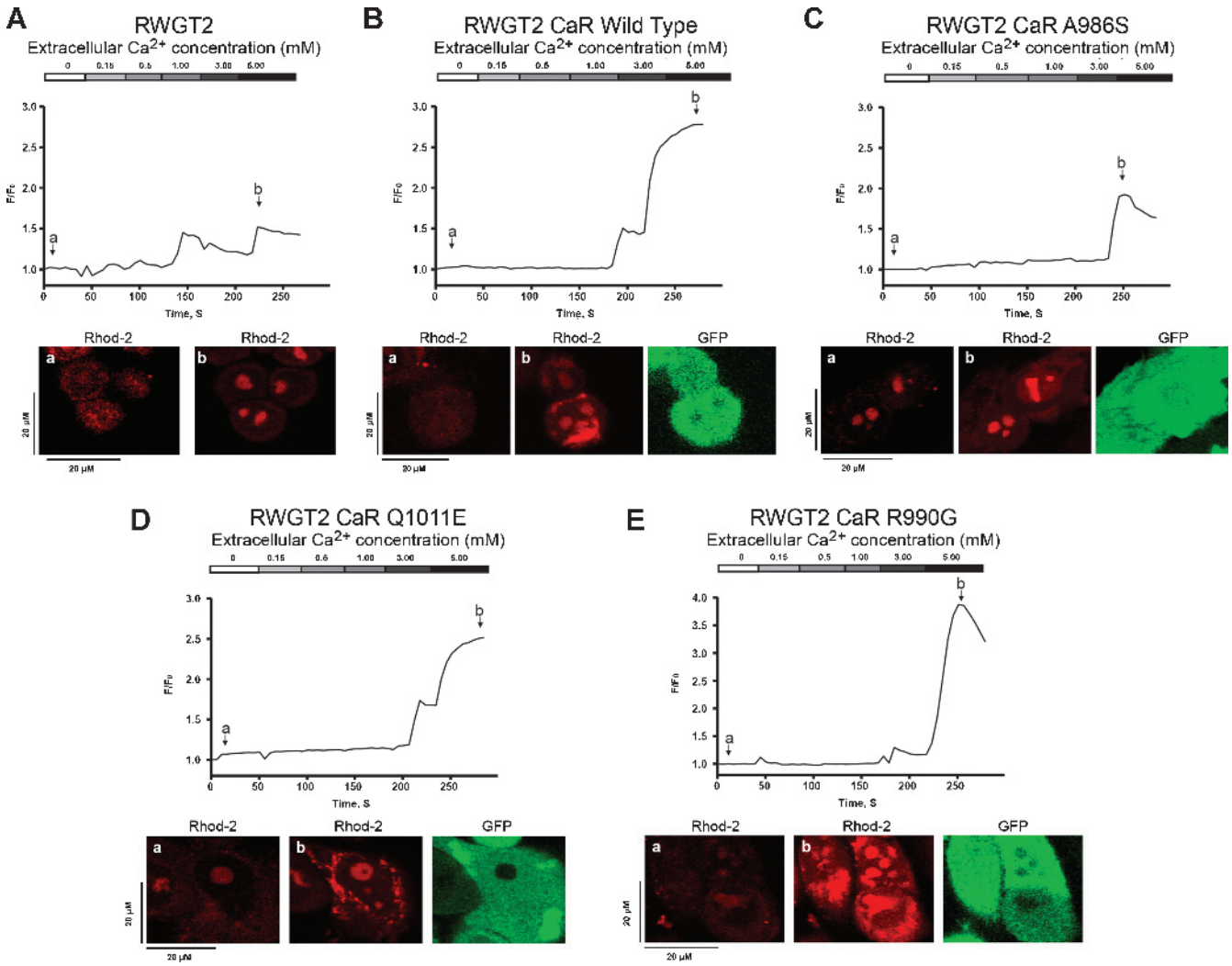

Figure 6. $Ca^{2+}{}_o$-stimulated $Ca^{2+}{}_i$ release in RWGT2 or RWGT2 transduced with CaR^{WT}, CaR^{A986S}, CaR^{Q1011E}, or CaR^{R990G}. (A–E) The graphs are representative of rhod-2 fluorescent $Ca^{2+}{}_i$ oscillations observed in RWGT2 and RWGT2 lines stably transduced with a GFP-expressing construct for either CaR wild-type receptor (CaR^{WT}) or the CaR mutations, CaR^{A986S}, CaR^{Q1011E}, or CaR^{R990G}. $Ca^{2+}{}_i$ baseline was measured in 0.0 mM Ca^{2+} bathing solution, and $Ca^{2+}{}_i$ oscillations were initiated by the addition of 0.15 mM Ca^{2+}. The panels below the $Ca^{2+}{}_i$ response curves labeled (a, b) are confocal microscopy images depicting rhod-2–loaded cells at baseline (a) and subsequent emittance of fluorescence on stimulation with $Ca^{2+}{}_o$ (b). The third panel in B to E depicts GFP expression from a GFP-CaR fusion protein.

of receptor signaling. Therefore, we examined CaR phosphorylation and the activation of downstream signal transduction pathways in the HARA line and the less $Ca^{2+}{}_o$-responsive BEN line. Regulation of PKC negative feedback induced by CaR^{T888} phosphorylation was examined in cell lysates from BEN and HARA cells at multiple time points using a custom-made polyclonal antibody raised to this epitope. Treatment of the HARA cells with 5.0 mM Ca^{2+} resulted in maximum CaR^{T888} phosphorylation at 60 minutes, whereas the maximum in the BEN cell line occurred at 5 minutes (Figure 5, *A* and *B*). This finding suggested that the negative feedback in the HARA CaR was delayed when compared to BEN.

To identify the molecular pathway involved in coupling PKC activation to CaR-activated PTHrP secretion, we used a human phosphoMAPK array to assess the relative level of phosphorylation of MAPKs in the BEN, HARA, and shRNA-CaR lines. The phospho-MAPK array detected strong phosphorylation of ERK1 (MAPK3), ERK2 (MAPK1), and JNK2 in both cell lines in response to Ca^{2+} stimulation as well as a decrease in the phosphorylation of both ERK1/2 in the companion shRNA-CaR lines (Figure W4, *A* and *B*). Thus, both ERK and JNK are activated to different extents in BEN and HARA lines.

We next examined the temporal activation of the ERK1/2, which has been implicated in mediating CaR post–receptor signaling and activation of PTHrP expression and secretion [21–23]. As shown in Figure 5*C*, ERK1/2 phosphorylation was increased in the HARA cell line at 5 minutes, whereas treatment of BEN required 10 minutes. ERK phosphorylation in the BEN cell line began to decrease at 15 minutes but persisted to 30 minutes in HARA. Thus, HARA seems to have prolonged activation of the MAPK pathway relative to BEN.

To further understand the basis of the altered CaR signaling in the HARA line, sequencing of genomic DNA for each cell type was performed. No mutations or SNPs were identified in the RWGT2 line. Interestingly, a homozygous missense SNP was identified in the

HARA (R990G) and BEN (Q1011E) lung SCC line, as well as a heterozygous SNP in HEK293T (A986S) cells (Figure W5*A* and Table W2*A*). All of the identified SNPs were located in exon 7 that encodes part of the cytoplasmic region of the receptor (Figure W5*B*). To follow up the cell line findings, the *CaR* gene was sequenced from nonaffected and affected lung tissues from 20 patients diagnosed with lung SCC. Surprisingly, the specific SNPs observed in the cell lines occurred in both the nonaffected and affected lung tissues in 6 (30%) of 20 patients (Table W2*B*). These findings raise the intriguing possibility that certain CaR SNPs may be associated with the development of lung SCC.

Functional Assessment of CaR SNPs

To characterize the functional properties of the CaR SNPs, we measured $Ca^{2+}{}_i$ oscillations after stimulation with $Ca^{2+}{}_o$ in RWGT2 cells transduced with lentiviral constructs containing the individual CaR wild-type (WT) and SNPs A986S, R990G, and Q1011E. Cells transduced with WT CaR had a threshold for a response to $[Ca^{2+}]_o$ between 3.0 and 5.0 mM, whereas this occurred between 1.0 and 3.0 mM in the nontransduced RWGT2. Overexpression of CaR^{WT} resulted in a two-fold increase and sustained release of $Ca^{2+}{}_i$ at 5.0 mM $Ca^{2+}{}_o$ (Figure 6, *A* and *B*). The overexpression and stimulation of the CaR^{A986S} in RWGT2 resulted in delayed $Ca^{2+}{}_i$ release occurring at 5.0 mM and was the least robust compared to the untransduced cell line (Figure 6, *A vs C*). Ectopic expression of CaR^{Q1011E} in RWGT2 produced a threshold response to $[Ca^{2+}]_o$ between 3.0 and 5.0 mM and also resulted in a more robust dose-response curve than CaR^{WT}. Overexpression of CaR^{R990G} in RWGT2 led to a maximum $Ca^{2+}{}_i$ release at 5.0 mM $Ca^{2+}{}_o$ with a 3.8-fold increase in fluorescence intensity, which represented the greatest $Ca^{2+}{}_i$ release (Figure 6*E*).

Because the *in vitro* functional assessment of the CaR^{R990G} variant suggested it had a gain-of-function in terms of activating signaling in response to high $[Ca^{2+}]_o$, we tested whether CaR^{R990G} expressed in a normocalcemic lung SCC model would induce a rapid onset of HHM. The overexpression of CaR^{WT} in the BEN line resulted in the development of HHM, whereas the vector-transduced lines did not (Figure 7*A*). A significant difference in time to onset of hypercalcemia was observed ($P < .001$) between BEN CaR^{R990G} and BEN CaR^{WT} (36 *vs* 49 days). Moreover, there were no differences in the mean tumor volume at the time of euthanasia. Average plasma PTHrP concentrations in the BEN CaR^{R990G} mice were 35% and 280% greater compared to the BEN CaR^{WT} and vector-transduced mice, respectively (Figure 7*C*). The results demonstrated that overexpression of CaR^{WT} was sufficient for the development of HHM in the BEN xenograft model, and the expression of CaR^{R990G} variant predisposed to an earlier onset of HHM.

Discussion

We have shown that lung SCCs express the CaR and that stimulation of CaR by $Ca^{2+}{}_o$ results in downstream activation of the MAPK pathway and up-regulation of PTHrP mRNA expression and secretion. In addition, CaR variants have been identified that, when ectopically expressed, alter $Ca^{2+}{}_i$ release. It seems that CaR is a critical factor for the rapid development of HHM because either overexpression of wild-type or CaR^{R990G} variant was sufficient to induce HHM in a normocalcemic lung SCC xenograft model. Therefore, $Ca^{2+}{}_o$ may act as an important stimulus to activate CaR in some lung SCCs.

The identification of CaR expression in lung SCC lines suggests a potential mechanism that contributes to abnormal calcium homeostasis in patients with lung SCC. The activation of PTHrP was largely abrogated in cells with shRNAs against CaR consistent with a role for the receptor in HHM rather than an indiscriminate effect of $[Ca^{2+}]_o$ on plasma membrane ion channels known to impact gene expression. Intriguingly, PTHrP expression and secretion were greatest at 3.0 mM Ca^{2+}, whereas toxic concentrations of Ca^{2+} (5.0 mM) decreased mRNA and secreted protein levels. Data show that the elevated serum Ca^{2+} concentrations as seen in HHM could stimulate

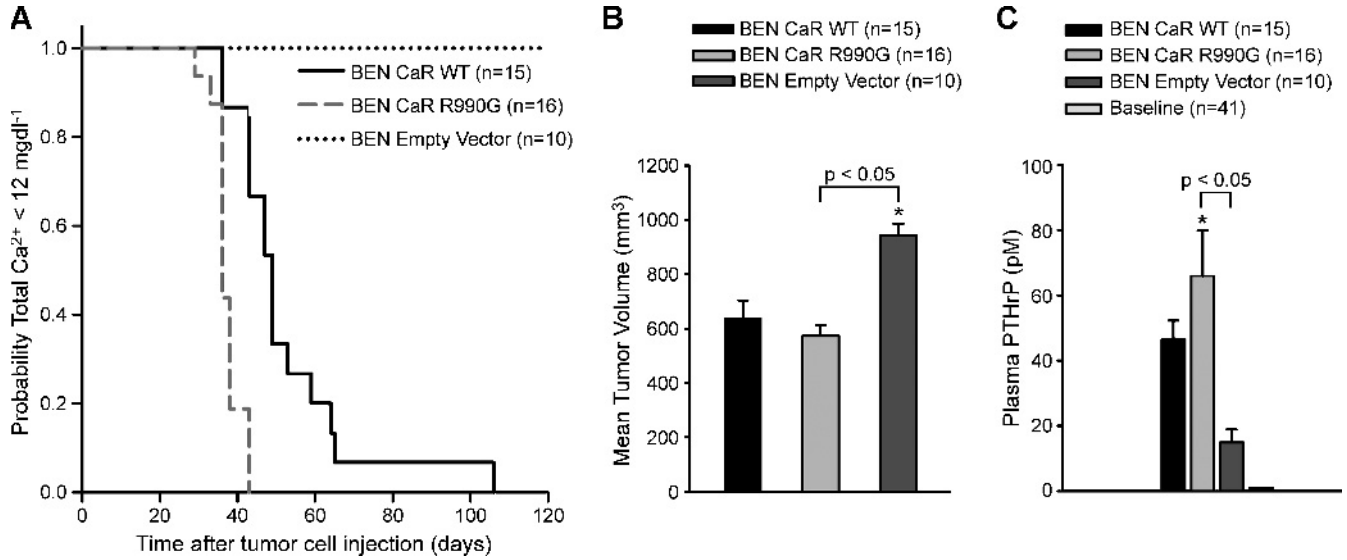

Figure 7. Xenograft models of BEN SCCs overexpressing either CaR^{WT}, CaR^{R990G} or the empty-vector. (A) Kaplan-Meier analysis indicated HHM developed more rapidly in BEN CaR^{R990G} than BEN CaR^{WT} ($P < .001$). (B) Tumor volume at the time of hypercalcemia ($P < .05$). (C) Comparison of plasma PTHrP in the mice with tumors. Mice with BEN CaR tumors were hypercalcemic, and mice expressing BEN empty-vector cells were not. Plasma PTHrP was measured before xenografting (baseline), at the time of development of HHM for the BEN CaR-bearing mice, and at the time of meeting early removal criteria for the BEN empty-vector xenografts.

CaR and provide a positive feedback loop to further activate PTHrP gene expression.

The use of shRNA to silence CaR expression permitted us to examine the role of the receptor in xenograft models of HHM. shRNA to CaR decreased PTHrP expression in SCC lines and confirmed the role of CaR in the activation of intracellular signaling, leading to increased PTHrP production. However, shRNA for CaR in HARA cells did not completely abrogate PTHrP expression or the ability to induce hypercalcemia *in vivo*. This is likely due to other humoral factors that contribute to PTHrP gene expression *in vivo* such as TNF-α, IL-1, IL-6, and/or stroma-derived cytokines. Transactivation of EGFR by CaR induction of membrane-associated matrix metalloproteinases, such as ADAM-17, has been reported in the HHM mice with PC-3 and Leydig H-500 cell lines [24,25]; however, we did not observe increased EGFR phosphorylation in HARA xenografts, suggesting that this mechanism did not significantly contribute to PTHrP production [3]. Alternatively, HHM may result from CaR signaling through $G\alpha_{q11}$ and PLC, which raises the possibility that PTHrP secretion could be induced by activation of other GPCRs that activate the ERK1/2 signaling pathway.

The identification of CaR SNPs in lung SCC demonstrates that receptor variants can influence signaling in cancer cells consistent with previous reports of receptor missense variants in endocrine diseases. The three identified SNPs encode missense amino acid changes (A986S, R990G, and Q1011E) in the C-terminus of CaR. Unfortunately, patients' serum calcium values at the time of diagnosis were not available for the samples from which the CaR was sequenced. We performed a functional analysis of the SNPs in a lung SCC line that had WT CaR because a cell line lacking the receptor remains to be identified. In our studies, RWGT2 cells transduced with the CaR^{R990G} SNP did not have an EC_{50} $Ca^{2+}{}_i$ release consistent with an activating mutation when compared to RWGT2 transduced with CaR^{WT}, although a greater release of $Ca^{2+}{}_i$ occurred at 5.0 mM. This suggested that variant receptor dimerization with the endogenous wild-type partially negated the gain-of-function observed for a homozygous R990G SNP in the HARA cell line. The R990G SNP of the *CaR* has been associated with primary hypercalciuria in patients with and without renal calculi [26,27]. Similar to our findings, Vezzoli et al. [26,28] suggest the 990G allele resulted in a gain-of-function of the *CaR* in HEK293 cells. Clinically, the presence of a heterozygous R990G variant in a lung cancer patient confirmed to have HHM would predict rapid progression of HHM once established, whereas a patient with a homozygous R990G SNP would likely develop HHM earlier because PTHrP production would be stimulated when serum Ca^{2+} was within the normal physiologic range. Finally, interpretation of our findings has been complicated because all published functional CaR studies have been performed in some derivative of HEK293 cells. It is quite possible that the previous conclusions about mutant CaR function have been influenced by the variants such as the A986S SNP present in the HEK293T cell line.

The role of CaR in disturbances of calcium homeostasis triggered by lung SCCs has led us to speculate on the potential therapeutic strategies directed at the receptor. Restoring normal CaR function may contribute to lessening the sequelae of cancer, particularly HHM, and could play a supporting role in cancer treatments. On the other hand, negative allosteric modulators (calcilytics) of the CaR, which decrease receptor activation, seem appealing for use in a patient with HHM. A potential limitation may be the lack of specificity for tumor-associated CaR, leading to unintended consequences such as stimulation of endogenous PTH secretion and renal calcium reabsorption with a resultant elevation or unchanged serum calcium concentration. In addition, the role of CaR variants on the function of these drugs may be important because mutations or SNPs may compromise allosteric binding sites for the inhibitors.

Acknowledgments

The authors thank Alan Flechtner and Florinda Jaynes for histological specimen processing and Tim Vojt for figure preparation. The authors declare no competing financial interests.

References

[1] Lazaretti-Castro M, Kayath M, Jamnik S, Santoro IL, Tadokoru H, and Vieira JG (1993). Prevalence of hypercalcemia in patients with lung cancer. *Rev Assoc Med Bras* **39**(2), 83–87.

[2] Gilmore JL, Gonterman RM, Menon K, Lorch G, Riese DJ, Robling A, and Foley J (2009). Reconstitution of amphiregulin–epidermal growth factor receptor signaling in lung squamous cell carcinomas activates PTHrP gene expression and contributes to cancer-mediated diseases of the bone. *Mol Cancer Res* **7**(10), 1714–1728.

[3] Lorch G, Gilmore JL, Koltz PF, Gonterman RM, Laughner R, Lewis DA, Konger RL, Nadella KS, Toribio RE, Rosol TJ, et al. (2007). Inhibition of epidermal growth factor receptor signalling reduces hypercalcaemia induced by human lung squamous–cell carcinoma in athymic mice. *Br J Cancer* **97**(2), 183–193.

[4] Berridge MJ, Bootman MD, and Roderick HL (2003). Calcium signalling: dynamics, homeostasis and remodelling. *Nat Rev Mol Cell Biol* **4**(7), 517–529.

[5] Davies SL, Ozawa A, McCormick WD, Dvorak MM, and Ward DT (2007). Protein kinase C–mediated phosphorylation of the calcium-sensing receptor is stimulated by receptor activation and attenuated by calyculin-sensitive phosphatase activity. *J Biol Chem* **282**(20), 15048–15056.

[6] Bai M, Trivedi S, and Brown EM (1998). Dimerization of the extracellular calcium-sensing receptor (CaR) on the cell surface of CaR-transfected HEK293 cells. *J Biol Chem* **273**(36), 23605–23610.

[7] Pollak MR, Brown EM, Chou YH, Hebert SC, Marx SJ, Steinmann B, Levi T, Seidman CE, and Seidman JG (1993). Mutations in the human Ca(2+)-sensing receptor gene cause familial hypocalciuric hypercalcemia and neonatal severe hyperparathyroidism. *Cell* **75**(7), 1297–1303.

[8] VanHouten J, Dann P, McGeoch G, Brown EM, Krapcho K, Neville M, and Wysolmerski JJ (2004). The calcium-sensing receptor regulates mammary gland parathyroid hormone–related protein production and calcium transport. *J Clin Invest* **113**(4), 598–608.

[9] Kohn EC and Liotta LA (1995). Molecular insights into cancer invasion: strategies for prevention and intervention. *Cancer Res* **55**(9), 1856–1862.

[10] Milara J, Mata M, Serrano A, Peiro T, Morcillo EJ, and Cortijo J (2010). Extracellular calcium-sensing receptor mediates human bronchial epithelial wound repair. *Biochem Pharmacol* **80**(2), 236–246.

[11] Ellison M, Woodhouse D, Hillyard C, Dowsett M, Coombes RC, Gilby ED, Greenberg PB, and Neville AM (1975). Immunoreactive calcitonin production by human lung carcinoma cells in culture. *Br J Cancer* **32**(3), 373–379.

[12] Hussain SR, Lucas DM, Johnson AJ, Lin TS, Bakaletz AP, Dang VX, Viatchenko-Karpinski S, Ruppert AS, Byrd JC, Kuppusamy P, et al. (2008). Flavopiridol causes early mitochondrial damage in chronic lymphocytic leukemia cells with impaired oxygen consumption and mobilization of intracellular calcium. *Blood* **111**(6), 3190–3199.

[13] Guise TA, Chirgwin JM, Taylor S, Boyce BF, Dunstan CR, and Mundy GR (1993). Deletions of C-terminal end of parathyroid hormone–related protein (Pthrp) have equivalent effects on bone and calcium homeostasis *in-vivo*. *J Bone Miner Res* **8**, S174.

[14] Iguchi H, Tanaka S, Ozawa Y, Kashiwakuma T, Kimura T, Hiraga T, Ozawa H, and Kono A (1996). An experimental model of bone metastasis by human lung cancer cells: the role of parathyroid hormone–related protein in bone metastasis. *Cancer Res* **56**(17), 4040–4043.

[15] Moseley JM, Kubota M, Diefenbach-Jagger H, Wettenhall RE, Kemp BE, Suva LJ, Rodda CP, Ebeling PR, Hudson PJ, Zajac JD, et al. (1987). Parathyroid hormone–related protein purified from a human lung cancer cell line. *Proc Natl Acad Sci USA* **84**(14), 5048–5052.

[16] Sanders JL, Chattopadhyay N, Kifor O, Yamaguchi T, Butters RR, and Brown EM (2000). Extracellular calcium-sensing receptor expression and its potential

role in regulating parathyroid hormone–related peptide secretion in human breast cancer cell lines. *Endocrinology* **141**(12), 4357–4364.

[17] Dolmetsch RE, Xu K, and Lewis RS (1998). Calcium oscillations increase the efficiency and specificity of gene expression. *Nature* **392**(6679), 933–936.

[18] Li W, Llopis J, Whitney M, Zlokarnik G, and Tsien RY (1998). Cell-permeant caged $InsP_3$ ester shows that Ca^{2+} spike frequency can optimize gene expression. *Nature* **392**(6679), 936–941.

[19] Hastings RH, Summerstorres D, Ditmer LS, Burton DW, Cheung TC, Spragg RG, Brown EM, and Deftos LJ (1995). Pulmonary alveolar epithelial-cells express a functional Pthrp-calcium–surfactant regulatory loop. *J Bone Miner Res* **10**, S382.

[20] Hastings RH, Duong HS, Burton DW, and Deftos LJ (1994). Alveolar epithelial-cells express and secrete parathyroid hormone–related protein. *Am J Resp Cell Mol* **11**(6), 701–706.

[21] Li X and Drucker DJ (1994). Parathyroid hormone–related peptide is a downstream target for Ras and Src activation. *J Biol Chem* **269**(9), 6263–6266.

[22] Aklilu F, Park M, Goltzman D, and Rabbani SA (1997). Induction of parathyroid hormone–related peptide by the Ras oncogene: role of Ras farnesylation inhibitors as potential therapeutic agents for hypercalcemia of malignancy. *Cancer Res* **57**(20), 4517–4522.

[23] Aklilu F, Gladu J, Goltzman D, and Rabbani SA (2000). Role of mitogen-activated protein kinases in the induction of parathyroid hormone–related peptide. *Cancer Res* **60**(6), 1753–1760.

[24] Tfelt-Hansen J, Yano S, John Macleod R, Smajilovic S, Chattopadhyay N, and Brown EM (2005). High calcium activates the EGF receptor potentially through the calcium-sensing receptor in Leydig cancer cells. *Growth Factors* **23**(2), 117–123.

[25] Yano S, Macleod RJ, Chattopadhyay N, Tfelt-Hansen J, Kifor O, Butters RR, and Brown EM (2004). Calcium-sensing receptor activation stimulates parathyroid hormone–related protein secretion in prostate cancer cells: role of epidermal growth factor receptor transactivation. *Bone* **35**(3), 664–672.

[26] Vezzoli G, Terranegra A, Arcidiacono T, Biasion R, Coviello D, Syren ML, Paloschi V, Giannini S, Mignogna G, Rubinacci A, et al. (2007). R990G polymorphism of calcium-sensing receptor does produce a gain-of-function and predispose to primary hypercalciuria. *Kidney Int* **71**(11), 1155–1162.

[27] Vezzoli G, Tanini A, Ferrucci L, Soldati L, Bianchin C, Franceschelli F, Malentacchi C, Porfirio B, Adamo D, Terranegra A, et al. (2002). Influence of calcium-sensing receptor gene on urinary calcium excretion in stone-forming patients. *J Am Soc Nephrol* **13**(10), 2517–2523.

[28] Vargas-Poussou R, Huang C, Hulin P, Houillier P, Jeunemaitre X, Paillard M, Planelles G, Dechaux M, Miller RT, and Antignac C (2002). Functional characterization of a calcium-sensing receptor mutation in severe autosomal dominant hypocalcemia with a Bartter-like syndrome. *J Am Soc Nephrol* **13**(9), 2259–2266.

[29] Dirksen WP, Mohamed SA, and Fisher SA (2003). Splicing of a myosin phosphatase targeting subunit 1 alternative exon is regulated by intronic *cis*-elements and a novel bipartite exonic enhancer/silencer element. *J Biol Chem* **278**(11), 9722–9732.

Supplemental Materials and Methods

Reagents

Spermine tetrahydrochloride was purchased from Sigma-Aldrich (St. Louis, MO). Mouse antihuman CaR monoclonal to amino acids (AA) 15-29 of the extracellular N-terminus (Sigma-Aldrich) was used for Western blot analysis. Adult normal human kidney whole-cell homogenates, normal human kidney lysate, and the secondary rabbit anti-mouse HRP antibody were purchased from Abcam, Inc. (San Francisco, CA). Phosphorylation of CaR residue Thr^{888} was studied using a custom-made rabbit polyclonal antibody to the phosphorylated form of Thr^{888}, which is within AA 882-896 of the human CaR sequence (KVAARA(pT)LRRSNVSR) (Invitrogen) [5]. For additional immunoblot studies, the following antibodies were used at a dilution of 1:000: anti–phospho-p44/42 MAP kinase (Thr202/Tyr204) no. 9101 and anti–p44/42 MAP kinase, GAPDH no. 2118 (Cell Signaling, Danvers, MA); and anti–β-actin was used at 1:5000 dilution (Sigma-Aldrich).

MTT Assay

A colorimetric assay (CellTiter 96 Non-Radioactive Cell Proliferation Assay; Promega, Madison, WI) was used according to the manufacturer's instructions to measure cell number and/or viability. Briefly, 5000 cells of each cell line were seeded in a 96-well culture plate in 100 μl of normal growth media and were incubated at 37°C in humidified 5% CO_2 for 24 hours. The following day, normal growth medium was replaced by 100 μl of $CaCl_2$-free DMEM supplemented with L-glutamine and 10% dialyzed FBS (0.15 mM Ca^{2+}). Calcium chloride was used as the active agent for $[Ca^{2+}]_o$ delivery and was added to the calcium-free DMEM to give final total calcium concentrations of 0.5, 1.0, 3.0, and 5.0 mM. The medium supplemented with the polycationic CaR agonist, spermine (2 mM), was used as a positive control. Twelve wells of each cell type were used for each $[Ca^{2+}]$ and spermine treatment. Cells were incubated with CaR agonist treatments at 37°C in humidified 5% CO_2 for 24 hours.

RNA Isolation and Quantitative Real-time RT-PCR

Total RNA was isolated from human lung tissue and lung SCC lines using the Absolutely RNA Miniprep Kit (Stratagene, La Jolla, CA) according to the manufacturer's instructions. The quality and quantity of the RNA were determined spectroscopically using a NanoVue Spectrophotometer (GE Healthcare, Piscataway, NJ). TaqMan Reverse Transcription kits (Applied Biosystems, Carlsbad, CA) were used to make cDNA for quantitative real-time PCR (QRT-PCR) analysis of all transcripts of PTHrP. The unlabeled primers and MGB FAM dye-labeled probe set for PTHrP QRT-PCR was from a Pre-Developed TaqMan Gene Expression Assay (Applied Biosystems). Absolute quantification was performed by interpolating quantities of unknown sample from a standard curve derived from known concentrations of PTHrP and GAPDH dilutions. Data were normalized by use of the ratio of the target cDNA concentration to GAPDH to correct for differences in RNA quantity between samples. The results represented in the figures were derived from experiments where the cDNAs were prepared at the same time and then analyzed by QRT-PCR performed on one plate when possible.

PTHrP Secretion Assays

For studying the effects of $Ca^{2+}{}_o$ and the polycationic CaR agonist, spermine, on PTHrP secretion, the three lung SCC lines and their respective shRNA-CaR lines were seeded in triplicate at a density of 3×10^6 cells/100 mm in polystyrene tissue culture dishes (Falcon, BD Biosciences, Bedford, MA) with 10 ml of normal growth medium. After 48 hours, the medium was removed from each plate, cells were washed with Dulbecco phosphate-buffered saline (DPBS), and the medium was replaced with 10 ml of sodium pyruvate and $CaCl_2$-free high-glucose DMEM (Invitrogen) supplemented with 10% dialyzed triple 0.1-μm sterile-filtered FBS (HyClone, Logan, UT) and 4 mM L-glutamine alone (0.15 mM) or supplemented with $CaCl_2$ to concentrations indicated in figures or 2 mM spermine. Medium-ionized $[Ca^{2+}]$ was confirmed using a calcium analyzer (Stat Profile Critical Care Xpress; Nova Biochemical, Waltham, MA). At times indicated after the addition of Ca^{2+} or spermine, the conditioned medium was removed and evaluated with two-site immunoradiometric assay (Diagnostic Systems Laboratories).

Immunoblot Analysis

For the measurement of CaR and actin proteins in lung SCC and HEK293T cells, cells were grown to 90% confluence in 100-mm dishes, subsequently placed on ice, rinsed with ice-cold DPBS, and lysed with a cold solution containing 20 nM HEPES (pH 7.4), 20 mM NaCl, 5 mM EDTA, 5 mM EGTA, 1 mM dithiothreitol, 0.5% Triton X-100, and protease inhibitors (Halt Protease Inhibitor Cocktail Kit; Pierce, Rockford, IL), 1 mM Na_3VO_4, 2 mM NaF, and 50 mM phenylmethanesulfonylfluoride. Cells were scraped, and the lysates were incubated in the buffer for 15 minutes on ice, and centrifuged for 20 minutes at 16,000*g* at 4°C. The supernatants were collected, and protein concentration was determined by a modified Bradford method (Bio-Rad Laboratories, Inc, Hercules, CA). For immunoblot analysis, 3× Laemmli sample buffer with 1 mM β-mercaptoethanol was added to 40 μg of protein extract (35-200 μg) at a final concentration of 33%, and the samples were heated at 100°C for 5 minutes. Cell protein extracts were fractioned on a precast 7% NuPAGE TRIS-acetate SDS gel (Invitrogen) followed by electrophoretic transfer to nitrocellulose membranes (Pall Life Sciences, Ann Arbor, MI). The membranes were incubated overnight (O/N) at 4°C with 0.2% Tween-20 in TBS and 2% bovine serum albumin with rabbit monoclonal and polyclonal antibodies. The blots were incubated with secondary antirabbit IgG horseradish peroxidase–linked antibody in 0.2% Tween-20 in TBS and 2% nonfat milk for 1 hour at room temperature (Cell Signaling). The custom phosphoCaR antibody was used at a 1:75 dilution. Immunoreactive bands were detected using a combination product that detects both chemiluminescence and fluorescence (Amersham ECL Plus Western Blot Detection Reagents, GE Healthcare Bio-Sciences).

Immunohistochemistry

Formalin-fixed paraffin-embedded tumor sections were placed on SuperFrost/Plus slides, deparaffinized in xylene, and rehydrated in an ethanol gradient. For PTHrP, a goat polyclonal anti–human PTHrP-(1-34) (sc-9680; Santa Cruz Biotechnology, Santa Cruz, CA) was used at a 1:50 dilution, and the secondary antibody was biotinylated rabbit anti-goat IgG (Vector Laboratories, Burlingame, CA) at a 1:200 dilution. For CaR, the custom phosphoCaR antibody was used at a 1:100 dilution, and the secondary antibody was biotinylated goat anti-rabbit used at 1:200 (Vector Laboratories). The specificity of the secondary antibodies was confirmed by the substitution of primary antibody with an irrelevant rabbit IgG1 or goat IgG1, by omission of the primary antibody and by the use of blocking peptide for PTHrP (sc-9680P;

Santa Cruz Biotechnology). Healthy adult human lung served as a positive control for phosphoCaR and PTHrP. A range of primary antibody dilutions were evaluated for phosphoCaR because this antibody had not been validated for immunohistochemistry.

Signaling Pathway Analysis

For the analysis of MAPK phosphorylation, a human Proteome Profiler antibody array was used according to the manufacturer's instructions (R&D Systems, Minneapolis, MN). The human phospho-MAPK antibody array is a nitrocellulose membrane with 21 different antikinase antibodies (Abs), including three positive controls and six negative controls, which are in duplicate. Positive controls are phosphorylated proteins, which are recognized by the antikinase Abs. BEN and HARA lung SCC lines and their respective shRNA-CaR SCC lines were seeded in duplicate at a density of 3×10^6 cells/100-mm polystyrene tissue culture dish (Falcon, BD Biosciences) in 10 ml of normal growth medium. After 24 hours, cells were washed twice with DPBS and the culture medium was replaced with 10 ml of a sodium pyruvate and calcium chloride–free high-glucose DMEM (Invitrogen) supplemented with 10% dialyzed triple 0.1-μm sterile-filtered FBS (HyClone) and 4 mM L-glutamine alone (0.15 mM) or supplemented with $CaCl_2$ to a final concentration of 3.0 mM for 30 minutes. Total protein from whole cells was harvested using Nonidet P-40 lysis buffer. Cell lysates were gently rocked for 30 minutes at 4°C and then centrifuged at 14,000*g* for 5 minutes (4°C). The supernatants were collected, and protein concentration was measured by the modified Bradford method (Bio-Rad Laboratories). A total of 300 μg of protein were used for each array. Arrays were developed by chemiluminescence (Amersham ECL Plus Western Blot Detection Reagents). The array immunoreactivity was quantified using Typhoon 9410 and ImageQuant TL Array Analysis software version 7 (GE Healthcare, Piscataway, NJ).

DNA Extraction

DNA from all lung SCCs and HEK293T cells was prepared using the DNeasy Blood and Tissue Kit (Qiagen, Valencia, CA) according to the manufacturer's instructions. General PCR conditions used to amplify *CaR* were an initial denaturation at 95°C for 2 minutes, 32 cycles of denaturation at 97°C for 30 seconds, annealing at 65°C for 60 seconds, and extension at 72°C for 1:30 minutes followed by elongation at 72°C for 7 minutes and termination at 4°C. All amplifications used a high-fidelity polymerase (Platinum Taq HiFi Polymerase; Invitrogen). Primers are listed in Table W2.

Extraction of DNA from Nonaffected and Lung SCC Tissue for Sequencing

Each patient had two lung biospecimens, one with nonaffected tissue (NAT) and the other an AJCC-staged lung SCC as determined by a board-certified pathologist. None of the patients had received chemotherapy or radiation therapy before acquisition of the tissue samples. For the analysis of mutations or SNPs in CaR, patients' tissues (SCC and the corresponding NAT for each patient) were pulverized with a mortar and pestle in liquid nitrogen, put in an Eppendorf tube with 180 μl of buffer ATL supplemented with 20 μl of proteinase K, placed in a thermomixer, and incubated at 56°C O/N. DNA was extracted and purified per manufacturer's instructions using the DNeasy Blood and Tissue Kit (Qiagen).

Sequencing

Standard PCR was used to generate high-fidelity *Taq* polymerase-amplified PCR products and subsequent sequencing. Amplicons were resolved on a 1% agarose gel to visualize the products. Each exon product was sequenced using BigDye Terminator Cycle Sequencing chemistry (Applied Biosystems). Sequencing reactions were run on an Applied Biosystems 3730 DNA Analyzer automated sequencer.

Sequence Alignment

The alignment was made using the Clustal W procedure in DNASTAR Software v MegAlign 5.06 (Madison, WI).

Plasmids and Site-Directed Mutagenesis for Generation of RWGT2 SNP Cell Lines

A construct containing the complete human CaR open reading frame (ORF) cloned into pCMV6-XL4 was purchased from OriGene Technologies, Inc, Rockville, MD (True Clone cat. no. SC119946; ref. ID: NM_000388). For site-directed mutagenesis, the CaR ORF was mutated using a strategy described previously [29] that involves PCR amplification of the entire pCMV6-XL4-CaR cDNA plasmid using the Expand Long Template PCR System (Roche, Indianapolis, IN). The oligonucleotides that contained the desired mutations were custom-synthesized, and these are listed in Table W1. A PCR product of appropriate size (~8.5 kb) was obtained for each mutation. The PCR products were blunt-ended with T4 DNA polymerase (New England Biolabs, Ipswich, MA), phosphorylated with T4 polynucleotide kinase (New England Biolabs), circularized with T4 DNA ligase (New England Biolabs), and transformed into DH5α cells. Once clones containing the desired mutations were obtained and confirmed by DNA sequencing, subregions of the mutated CaR ORFs were subcloned back into the pCMV6-XL4-CaR cDNA parent plasmid to remove any unwanted mutations elsewhere in the plasmid that may have been caused by *Taq* DNA polymerase errors. The complete wild-type and mutated CaR ORFs were then subcloned as 3571-nucleotide *Psh*AI-*Not*I fragments into the *Swa*I-*Not*I sites of the GFP-expressing lentiviral vector pCDH-CMV-MCS-EF1-copGFP (System Biosciences, Mountain View, CA). Finally, a fusion protein between the wild-type/mutant CaR ORFs and GFP was genetically engineered by replacing the CaR stop codon with a *Not*I restriction site. This modified CaR 3′-end was cloned into the lentiviral vectors as a 517-nucleotide *Bam*HI-*Not*I fragment replacing the 751-nucleotide *Bam*HI-*Not*I fragment containing the wild-type CaR 3′-end. The entire CaR ORFs of the final lentiviral vectors were confirmed by DNA sequencing. Generation of wild-type and variant CaR expression vectors was initiated by cloning constructs into the pCDH-EF1-MCS-T2A-copGFP reporter vector (Systems Biosciences). pCDH cDNA CaR wild-type and mutant constructs were subsequently packaged into VSV-G pseudotyped lentiviral particle supernatant (Cincinnati Children's Hospital Medical Center Viral Vector Core, Cincinnati, OH). BEN and RWGT2 cells were seeded at a density of 5×10^5 cells/6-mm well and incubated O/N at 37°C. Twenty-four hours later, viral supernatant of each mutant and wild-type construct with a MOI of 5, polybrene 8 μg/ml, and DMEM + 10% FBS were added to each well to a total volume of 2 ml. Spinoculation was performed at 32°C for 1 hour at 2700 rpm. Transduced cells expressed visible GFP within 48 hours and were selected by FACS analysis.

Table W1. Human-Specific Primers for CaR.

Primer Set	Forward	Reverse
Human-specific primers used for calcium-sensing receptor PCR amplification of exon gDNA		
CaR Exon 2	5′-AGTCTGCCACCCCTAGGCCC-3′	5′-TGCGTTTGGTGCAGCTTTTCTCCA-3′
CaR Exon 3	5′-ACAGAGCATGCCATGAAGCCAGAG-3′	5′-GCACCCCCAAGCCTGCTTCT-3′
CaR Exon 4	5′-GCCACCTCCACAACAGCCTGG-3′	5′-TGGAGTTGCAGCCCAACTCTGC-3′
CaR Exon 5	5′-TGTGCAGGGCACAGCCTACCT-3′	5′-TGTGCAGGGCACAGCCTACCT-3′
CaR Exon 7A	5′-CCCACCACCACATGTACACTCACA-3′	5′-GCACGCCAGCAAGCCAAAGC-3′
CaR Exon 7B	5′-GCTTTGGCTTGCTGGCGTGC-3′	5′-TCAGAGGAAAGGAGTCTGGGGCG-3′
Primers used for site-directed mutagenesis (mutated nucleotides are underlined and bolded)		
A986S	5′-CCCACAGGAATTCTACGCACCAGA-3′	5′-CCATGG**A**GTTCTTCTGAGGCTCATC-3′
R990G	5′-CCAC**G**GGAATTCTACGCACCAGA-3′	5′-GCCATGGCGTTCTTCTGAGG-3′
Q1011E	5′-CAC**G**AGCCATTACTCCCGCTG-3′	5′-TCGGGTCAGCGTATCGCTGCTT-3′
Human-specific primers used for the amplification of the 481-bp calcium-sensing receptor PCR product		
CaR	5′-CGGGGTACCTTAAGCACCTACGGCATCTAA-3′	5′-GCTCTAGAGTTAACGCGATCCCAAAGGGCTC-3′
Human-specific primers used for the amplification of the 176-bp GAPDH PCR product		
GAPDH	5′-TGCACCACCAACTGCTTAG-3′	5′-GAGGCAGGGATGATGTTC-3′

Table W2. (A) Cell Line SNPs and (B) Human Nonaffected and Lung SCC Tissue SNPs.

(A)

Domain	Cell Line	Amino Acid Change	Exon	Codon Change	Genotype	Other
	RWGT2	None				
Cytoplasmic	HEK293T	A986S	7	GCC → UCC	Heterozygous	Polymorphism
	HARA	R990G	7	AGG → GGG	Homozygous	Polymorphism
	BEN	Q1011E	7	CAG → GAG	Heterozygous	Polymorphism

(B)

Domain	Age, Sex, and Race*	Amino Acid Change	Exon	Codon Change	Genotype	$N^{\dagger}$	Tissue[‡]	Other
Cytoplasmic	69Y/M/Caucasian 72Y/M/Caucasian 74Y/F/Caucasian	A986S	7	GCC → UCC	Heterozygous	3	NAT and SCC	Polymorphism
	59Y/M/Caucasian	R990G	7	AGG → GGG	Heterozygous	1	NAT and SCC	Polymorphism
	68Y/F/Caucasian 72Y/F/Black	Q1011E	7	CAG → GAG	Heterozygous	2	NAT and SCC	Polymorphism

*F indicates female; M, male; Y, years old.
†*N*, number of individuals affected with SNP from a total of 20 patients.
‡NAT indicates nonaffected pulmonary tissue; SCC, squamous cell carcinoma.

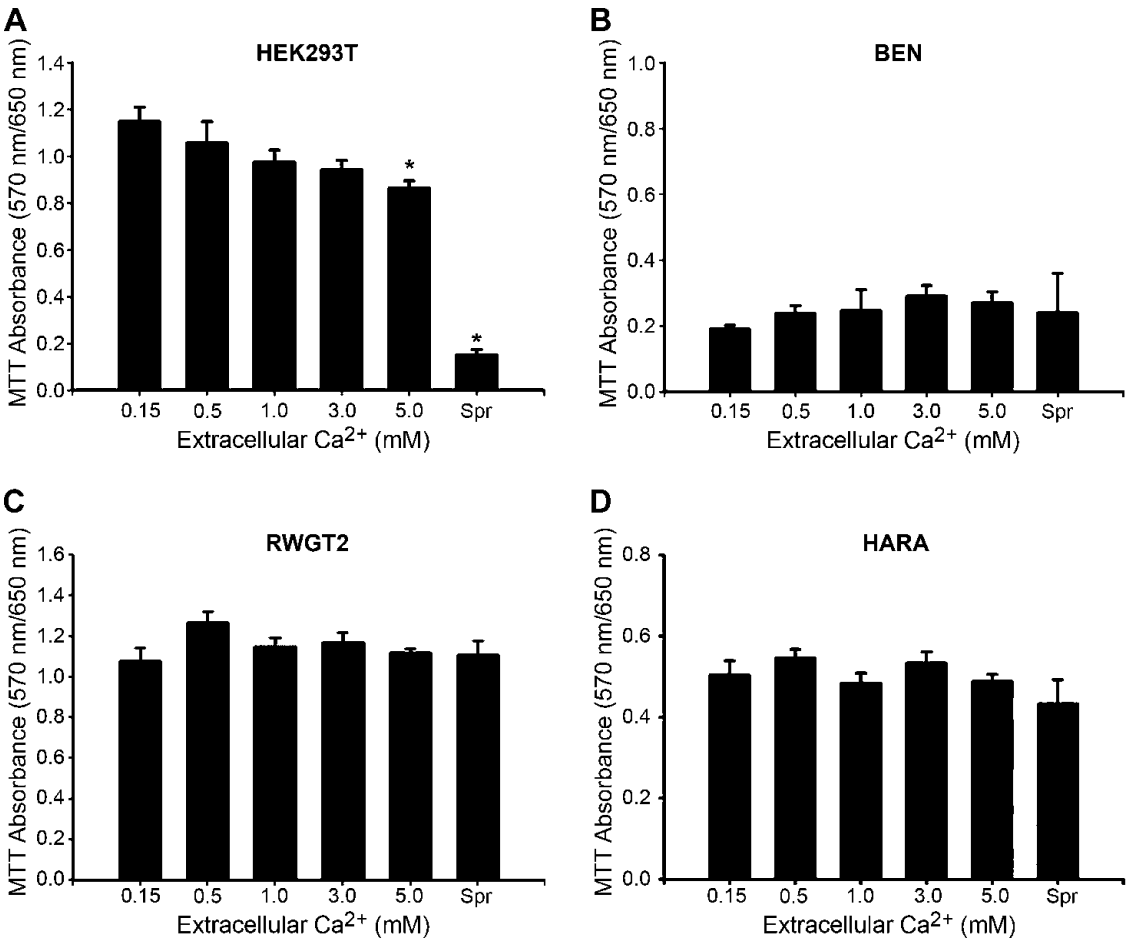

Figure W1. Extracellular calcium concentrations decreased cell viability in HEK293T cells but not lung SCCs. (A–D) MTT assays were used to measure the cytotoxicity of $Ca^{2+}{}_o$ and 2 mM spermine on HEK293T and lung SCC lines after 24 hours of treatment (*$P < .05$ *vs* 0.15 mM). There were no significant effects on cell viability of any of the lung SCCs (B–D); however, a dose-response decrease in cell viability occurred in the HEK293T cells.

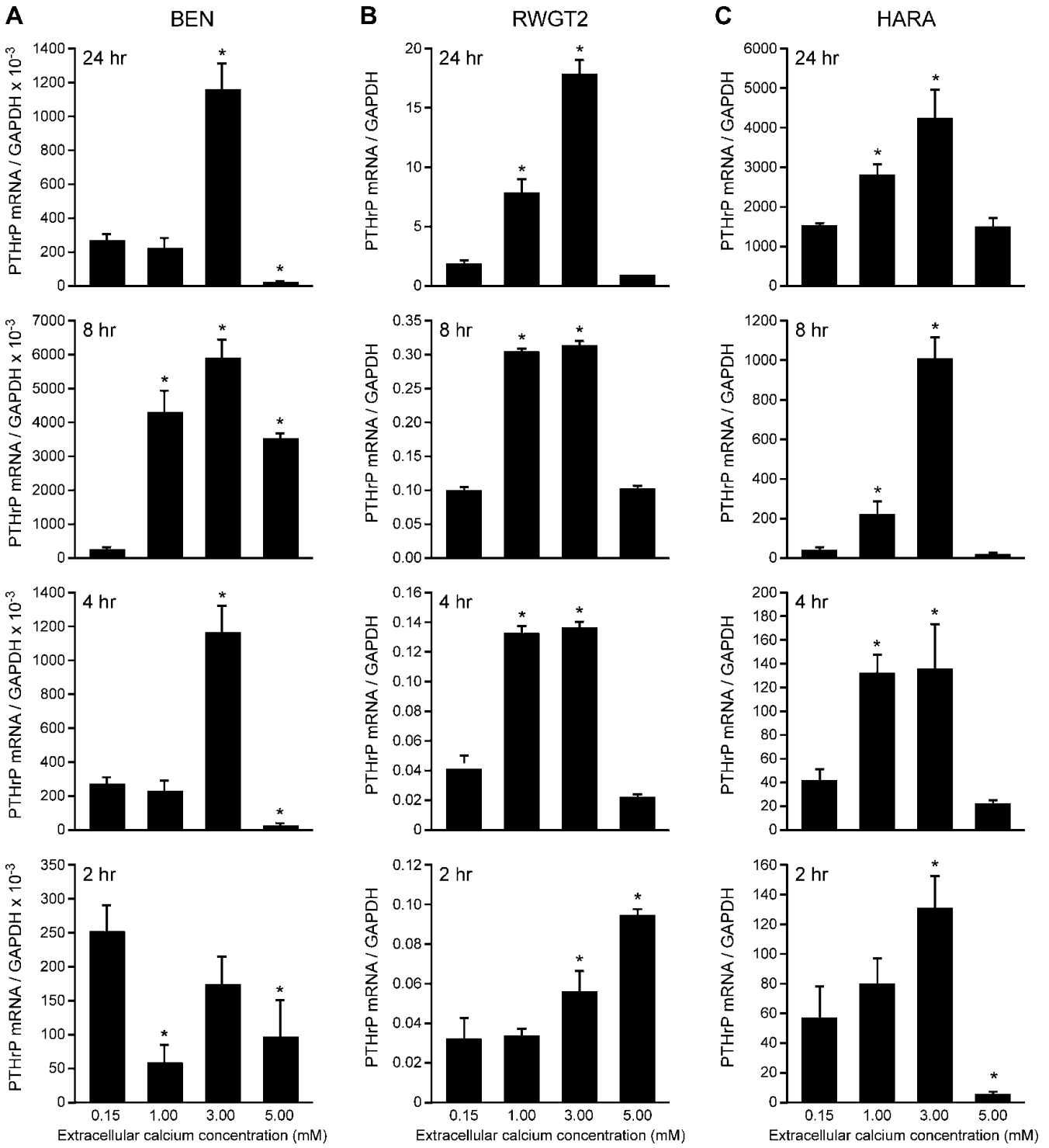

Figure W2. Escalating [Ca^{2+}_o] increased PTHrP mRNA levels of lung SCC lines as measured by quantitative real-time RT-PCR. (A–C) Addition of 3.0 mM Ca^{2+} to lung SCC cultures for 2, 4, 8, and 24 hours resulted in significant increases in PTHrP/GAPDH mRNA ratios compared with controls (0.15 mM) at all time points in all cell lines except BEN at 2 hours. The relative ratios of PTHrP mRNA to GAPDH mRNA levels were expressed as mean ± SEM of three cultures per time point and concentration (*$P < .05$ *vs* 0.15 mM).

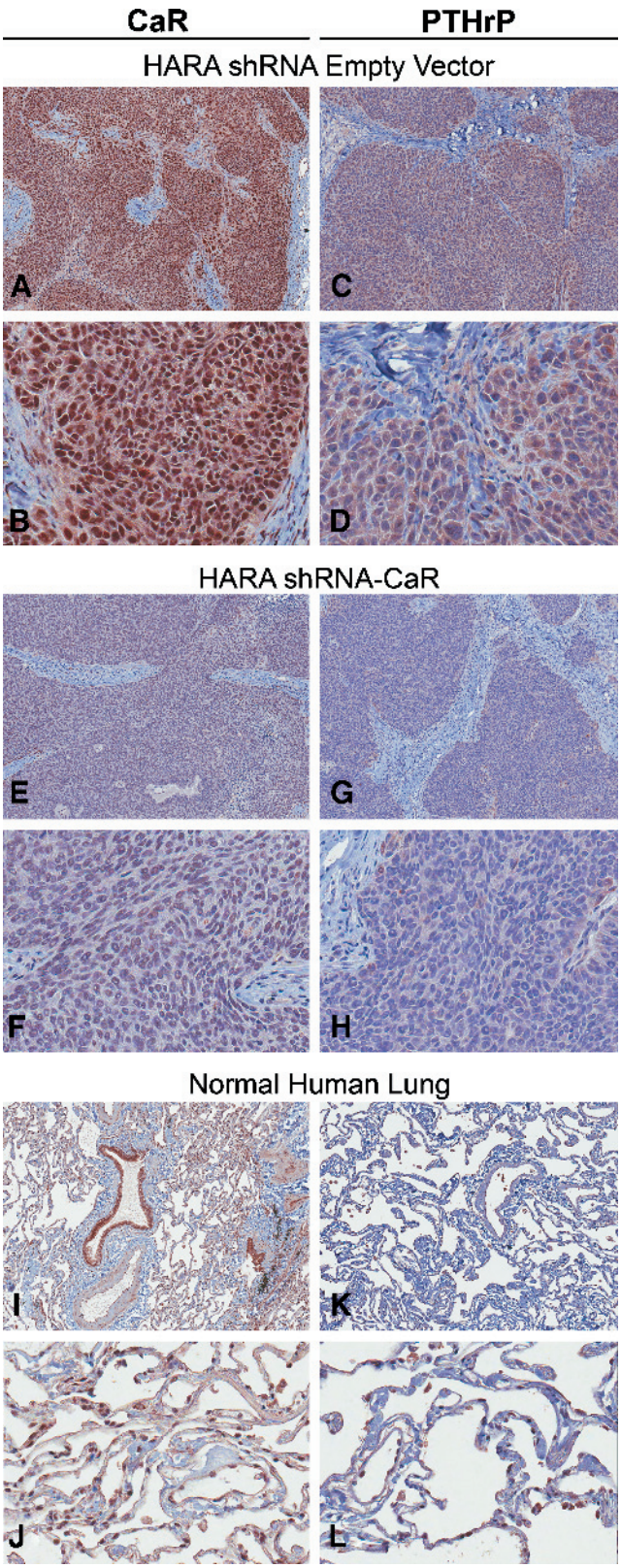

Figure W3. Immunohistochemistry detection of phosphoCaR and PTHrP expression in tumors from HARA shRNA empty-vector and HARA shRNA-CaR xenograft models of HHM. Immunohistochemistry for phosphoCaR is represented by panels on the right. PTHrP immunohistochemistry is represented by panels on the left. HARA shRNA empty-vector lung SCC (A–D). (A) Low-power magnification revealing diffuse intense phosphoCaR staining of the nuclei and cytoplasm of individual lung SCC cells, and nuclear staining of the fibroblasts and endothelial cells of the tumor stroma. Magnification, ×50. (B) Higher magnification of A, ×400. (C) Low-power magnification showing marked diffuse granular PTHrP staining in the cytoplasm with faint staining occasionally localized to the nucleus in addition to the cytoplasm. Nuclei of fibroblasts in the stroma demonstrate light PTHrP staining. Magnification, ×50. (D) Higher magnification of C, ×400. HARA shRNA-CaR lung SCC (E–H). (E) Low-power magnification of lung SCC revealing very light phosphoCaR staining of the nuclei and minimal staining of the cytoplasm (A *vs* E). Magnification, ×50. (F) Higher magnification of E, ×400. (G) Low-power magnification showing decreased PTHrP-positive staining of the cytoplasm and minimal staining of the nuclei (G *vs* C). (H) Higher magnification of G, ×400. Normal adult human lung tissue (I–L). (I) Low-power magnification of phosphoCaR protein expression was located in the epithelium of the bronchus and the smooth muscle of the pulmonary artery. Magnification, ×50. (J) Higher magnification showed phosphoCaR-positive staining in the endothelial cells of the pulmonary venule and type 2 pneumocytes. (K) PTHrP-positive staining was present in the endothelial cells of pulmonary arteries. Magnification, ×50. Higher magnification detected PTHrP staining in type 2 pneumocytes and in capillary and venule endothelium, ×400.

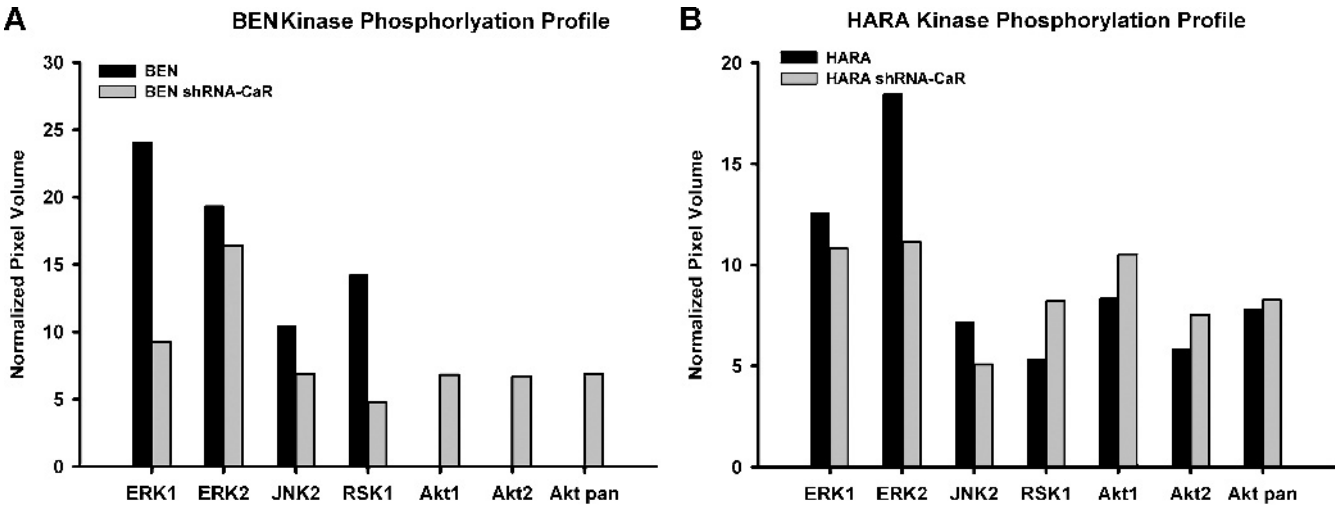

Figure W4. Stimulation of CaR with 3.0 mM Ca^{2+} activated both ERK1/2 and JNK2 MAPK modules in the BEN and HARA lung SCC lines. The human phospho-MAPK array was used to detect multiple phosphorylated kinases in human lung SCCs with either an intact CaR or a silenced CaR after stimulation with Ca^{2+}. BEN, BEN shRNA-CaR and HARA, HARA shRNA-CaR cells, 3×10^6 cells/100-mm plate were seeded in duplicates and grown until ~80% confluent. Twenty-four hours after seeding, growth medium was changed to 0.15 mM calcium-free DMEM supplemented with 10% dialyzed FBS and L-glutamine for 4 hours. Cells were washed with DPBS, and medium was changed to DMEM with 3.0 mM Ca^{2+}, 10% dialyzed FBS, and L-glutamine for 30 minutes. Cells were harvested. Arrays were incubated with 300 μg of cell lysate and were performed in duplicate. A and B depict the phosphorylation profile of BEN and HARA lines as represented by normalized pixel volumes.

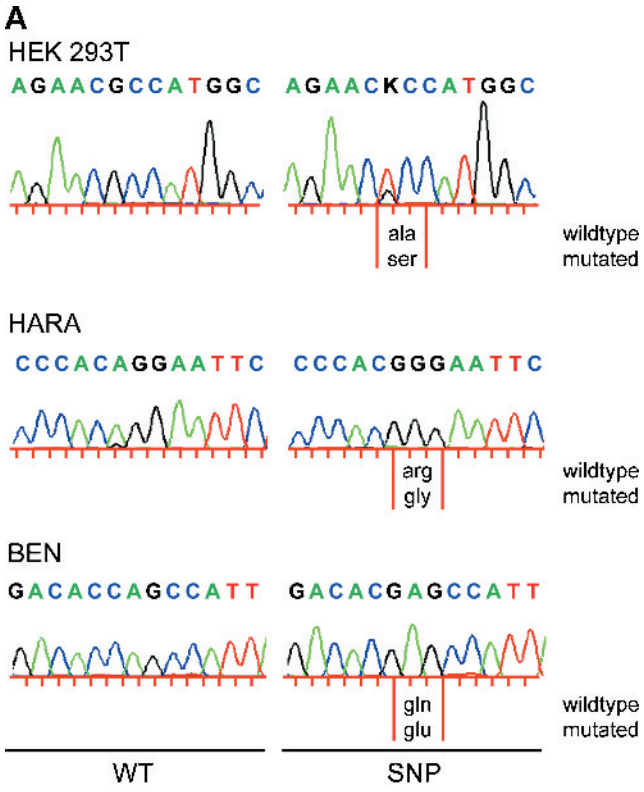

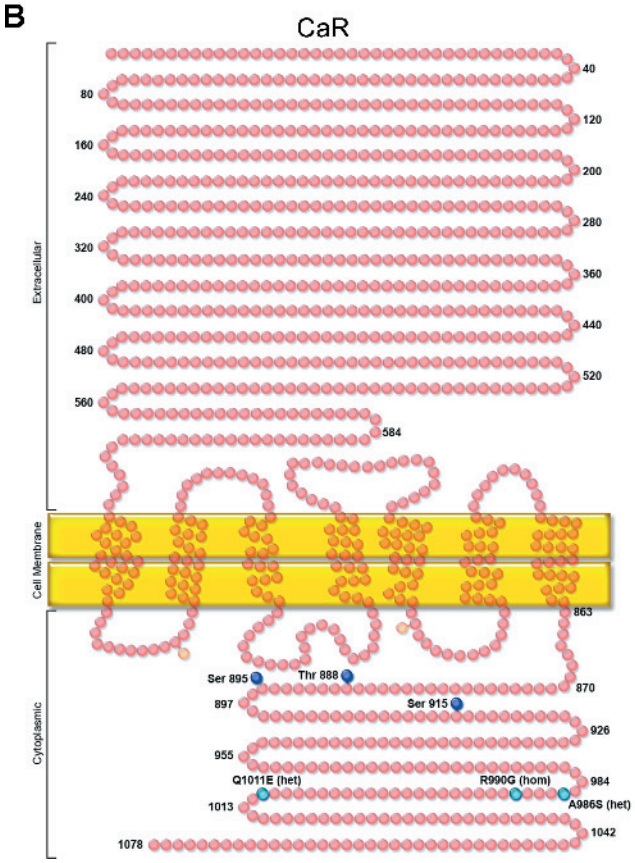

Figure W5. DNA sequence analysis CaR in lung SCC and HEK293T cell lines and a schematic of the CaR demonstrating the locations of SNPs and three PKC phosphorylation sites with known receptor regulation. (A) DNA sequence analysis of CaR showing the nucleotide sequence of wild-type CaR on the left and the sequence with the identified CaR SNP on the left. The corresponding amino acid changes are represented below the changed nucleotide sequence. (B) Topographical representation of the human CaR showing the position of the identified SNPs in lung SCC and HEK293T cell lines. Individual amino acids are represented by red circles; light blue circles represent SNPs. Heterozygous or homozygous SNPs are denoted (het) and (hom), respectively. Dark blue circles represent PKC phosphorylation sites known to regulate CaR activity. Pale orange circles represent two additional putative PKC phosphorylation sites with unknown activity.